

Article

Low Temperature Cu/Ga Solid–Liquid Inter-Diffusion Bonding Used for Interfacial Heat Transfer in High-Power Devices

Guoqian Mu , Wenqing Qu *, Haiyun Zhu, Hongshou Zhuang and Yanhua Zhang *

School of Mechanical Engineering and Automation, Beihang University, Beijing 100191, China; mgqapple@buaa.edu.cn (G.M.); zhuhaiyun@buaa.edu.cn (H.Z.); hzhuang@buaa.edu.cn (H.Z.)

* Correspondence: quwenqing@buaa.edu.cn (W.Q.); zhangyh@buaa.edu.cn (Y.Z.); Tel.: +86-10-82317702 (W.Q.)

Received: 29 July 2020; Accepted: 1 September 2020; Published: 10 September 2020



Abstract: Interfacial heat transfer is essential for the development of high-power devices with high heat flux. The metallurgical bonding of Cu substrates is successfully realized by using a self-made interlayer at 10 °C, without any flux, by Cu/Ga solid-liquid inter-diffusion bonding (SLID), which can be used for the joining of heat sinks and power devices. The microstructure and properties of the joints were investigated, and the mechanism of Cu/Ga SLID bonding was discussed. The results show that the average shear strength of the joints is 7.9 MPa, the heat-resistant temperature is 200 °C, and the thermal contact conductance is 83,541 W/(m²·K) with a holding time of 30 h at the bonding temperature of 100 °C. The fracture occurs on one side of the copper wire mesh which is caused by the residual gallium. The microstructure is mainly composed of uniform θ -CuGa₂ phase, in addition to a small amount of residual copper, residual gallium and γ_3 -Cu₉Ga₄ phase. The interaction product of Cu and Ga is mainly θ -CuGa₂ phase, with only a small amount of γ_3 -Cu₉Ga₄ phase occurring at the temperature of 100 °C for 20 h. The process of Cu/Ga SLID bonding can be divided into three stages as follows: the pressurization stage, the reaction diffusion stage and the isothermal solidification stage. This technology can meet our requirements of low temperature bonding, high reliability service and interfacial heat transfer enhancement.

Keywords: heat dissipation; interfacial heat transfer; SLID; Cu/Ga; low temperature bonding; thermal interface material (TIM)

1. Introduction

With the increasing power dissipation and shrinking feature sizes of high-power devices (such as insulated gate bipolar translator, central processing unit, laser load devices, etc.), the heat generated is gradually increasing. High temperature has a bad impact on the performance of power devices. Research shows that the device failure rate doubles and the lifespan of the devices is halved for every 10 °C rise in the joining temperature [1], and that more than 55% of the failures of electronic devices are caused by too-high temperatures [2]. Therefore, high requirements for heat dissipation are established [3], and some efficient heat sinks (such as heat pipe, microchannel, refrigeration chip, etc.) have been developed. As such, the interfacial heat transfer between heat source and heat sink is becoming a severe bottleneck, currently limiting the further scaling of performance. Meanwhile, the heat flux density through the interface is constantly increasing [4], so interfacial heat transfer enhancement is essential for the development of high-power devices. The common methods used currently are as follows: adding thermally conductive particles (i.e., metals, ceramics) to nonmetallic thermal interface materials (TIM) [5] and using low melting temperature alloy (LMTA) [5], etc. However, the thermal conductivity of nonmetallic materials is lower than that of metallic materials, and thermal

greases are easy to age. The LMTA and some nonmetallic TIM are in the liquid state in the service process, and are easy to flow out, which affects the reliability negatively [6], and external pressure is needed for them [5,6]. Thus, the metallurgical bonding of mating surfaces is the best choice for interfacial heat transfer enhancement.

Considering the special working conditions of some power devices, they must be assembled at low temperatures. For example, the aluminum ammonia heat pipe must be assembled under 95 °C, and the laser generator cannot exceed 80 °C. At the same time, they often work at a temperature that is close to or even higher than the bonding temperature. Therefore, the reliability of the bonded surfaces will not decrease at higher temperatures. At present, the methods that can be used for low-temperature bonding with high reliability include nanoparticle sintering technology, transient liquid phase sintering (TLP) and solid-liquid inter-diffusion bonding (SLID), etc.

Nanoparticle sintering technology can meet the above requirements, and the electrical and thermal conductivity [7,8] and mechanical properties [9–11] of the joints are excellent. However, its bonding temperature is generally higher than 200 °C [12], which is still too high for many power chips or devices. The interfacial microstructure has significant porosity, which will reduce the thermal and mechanical properties of the joints [13]. Besides, this technology costs a lot, given the high price of Ag. Its microstructure and properties cannot be improved under the action of high service temperature, and they will deteriorate at high temperatures and with long-term service.

Therefore, metallurgical bonding with a uniform interfacial microstructure is an important solution to this problem. The TLP sintering used mostly in the microelectronic packaging industry, also known as SLID [14], is a good way to solve this problem. It uses a high melting point metal and a low melting point metal to form intermetallic compounds (IMC), which melt at higher temperatures than the bonding temperature during isothermal solidification [15].

In this paper, the low temperature metallurgical bonding of copper substrates is investigated. The Cu substrates were successfully bonded with a self-made interlayer at 100 °C without any flux. Then, the microstructure, shear strength, temperature resistance and thermal contact conductance of the joints were studied, and the mechanism of Cu/Ga SLID bonding was discussed.

2. Materials and Methods

In this paper, we chose Ga as the low melting point metal, for the melting point of Ga (29.75 °C) is lower than Sn (231.9 °C) and In (156.6 °C), and the processing temperature of Ga-based solder is lower. Besides, gallium has excellent wetting properties and can decrease melting temperature, and so on. [16,17]. Although the eutectic points of Ga-Sn and Ga-In are lower than the melting point of Ga, the bonding temperature of Ga-based solder can completely meet our requirements. Besides, more work needs to be done on the interaction between Ga-based solder and components at low temperatures to fully utilize this kind of interesting material, and expedite its use in industry [17].

Cu substrates are utilized via their widespread use as metallization materials [18]. We chose Cu as the high melting point metal. The Au/Ga system has been investigated [19], as has the very high diffusion speed of gold into liquid Ga during the process expediting the extreme formation of Kirkendall voids. The solderability of the Ag/Ga system is poor. The inter-diffusion coefficient of Cu/Ga is appropriate [20], but the Cu/Ga system has been rarely used, and they often introduce Au or Pt as a seed layer [21,22].

Cu/Ga solder paste and copper wire mesh attached with liquid Ga were used to prepare the self-made interlayer. Copper wire mesh plays the role of skeleton, which can help keep the thickness of the interlayer uniform. The Cu content in the interlayer was optimized to be about 33 wt. %, corresponding to the stoichiometry of the main reaction of copper with gallium at a small copper excess. In the whole bonding process, gallium is in the liquid state, and solid copper is surrounded by a liquid, which greatly shortens the atom diffusion distance and makes Cu/Ga inter-diffusion easy. The requirement of the substrate roughness and flatness is not high.

The copper wire mesh is pure copper, with a purity of 99.9%, 400 mesh and diameter of 40 μm . The particle size of the copper powder is 300 mesh. The purity of gallium is 99.9%. The size of the copper substrate is 60 mm \times 10 mm \times 1.5 mm. The materials were provided by the China General Research Institute of Nonferrous Metals. The copper substrate and copper wire mesh will be pretreated to remove the oil and oxide film on surface before joining.

Bonding process: (1) Coat the copper wire mesh with liquid Ga uniformly at 40 $^{\circ}\text{C}$; (2) Prepare the Cu/Ga solder paste at 40 $^{\circ}\text{C}$. Ga exists in a liquid state at 40 $^{\circ}\text{C}$ and has excellent wettability, so copper powder can be wetted by liquid Ga completely without any flux to obtain silver white Cu/Ga solder paste; (3) Apply Cu/Ga solder paste on the surface of the Cu substrates uniformly; (4) Place the copper wire mesh attached with liquid Ga between the two Cu substrates in fixture with pressure of 2 MPa; (5) Subsequently, the assembled samples are held in the furnace at 100 $^{\circ}\text{C}$ for 10 h, 20 h and 30 h respectively; (6) Take out the samples from the furnace for further observation and testing. Figure 1 shows the schematic diagram of the bonding process.

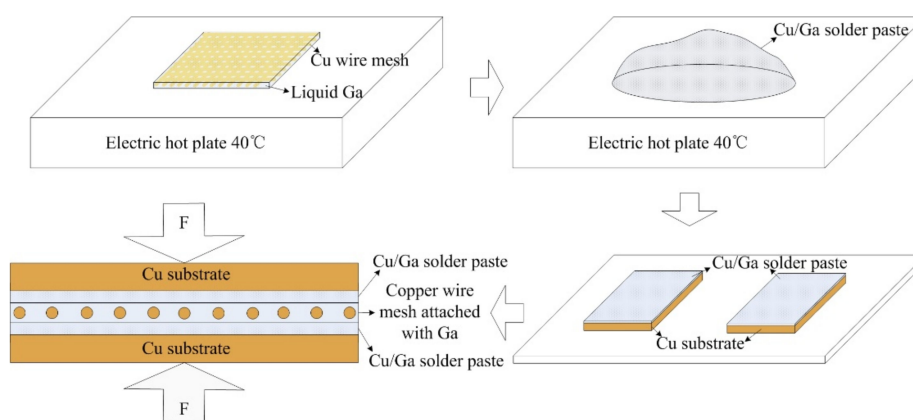


Figure 1. The schematic diagram of the bonding process.

An optical microscope (OM) (Olympus B \times 5) and a scanning electron microscope (SEM) (JSM-7500) were used to investigate the interfacial microstructure of the joints. The phase constitutions of the intermediate layer were analyzed by X-ray diffraction (XRD) tests with with X-ray diffractometer (D/Max-2200pc). The X-ray source is excited by the copper target. The working voltage and current were 40 kV and 40 mA, respectively, and the scanning speed was set at 6 degrees per minute. Micro-area composition analysis was investigated via Energy dispersive spectrometry (EDS) detected with SEM. The EDS analysis was performed with an acceleration voltage of 20 kV. Firstly, the joints were cut and fixed with bakelite power to make metallographic specimens. The specimens were ground with 260, 800, 1200 and 2000 waterproof abrasive paper, and then polished with 2 μm and 0.5 μm diamond paste. The XRD and SEM tests were conducted first, and etching was performed before the OM tests.

The mechanical properties of the joints were evaluated by shear testing at room temperature using a tensile testing machine (MTS50KN) with a machine displacement rate of 0.5 mm/min. The average shear strength of five joints was used to contrast the mechanical property. The joint used was the lap joint, and the lap length was 5 mm. If the tension center and the sample center are not in a straight line, the test results will be inaccurate. Two small pieces were bonded at both ends of the lap joint, as shown in Figure 2. When holding the samples on the fixture of the testing machine, attention should be paid to the position of the samples so as to prevent eccentricity.

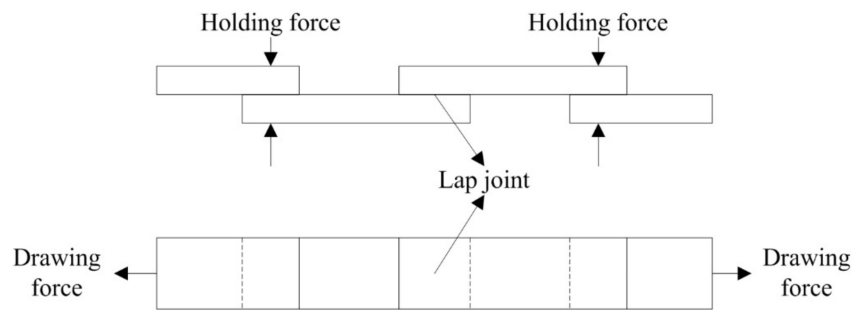


Figure 2. Schematic diagram of shear test specimen.

The method of the temperature resistance test is the weight method. A certain load is applied to the specimen, and then the specimen is heated to a predetermined temperature to observe whether the joint is remelted at this temperature. The test was carried out in a resistance furnace, and holes were punched on each piece of the lap joint respectively to hang the weight of 50 g, as shown in Figure 3. After several minutes, the specimens reached the preset temperature of 200 °C. The specimens were hold at this temperature for 10 min to observe the joints.

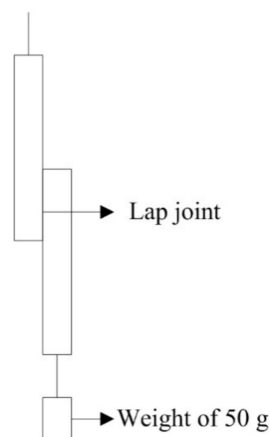


Figure 3. Schematic diagram of the temperature resistance test.

The thermal property is evaluated by the thermal contact conductance of the bonded interface, using infrared-assisted steady state temperature measurement of the vacuum thermocouple. The rated heat flux (q) was selected as 10, 50, 100, 200 and 300 W/cm², and the simulation device for the test was designed according to the basic law of heat conduction (Fourier law), as shown in Figure 4. The material was copper, and the thermal conductivity of Cu is 427 W/(m·K) [6]. The whole device was wrapped with multi-layer thermal insulation material and put into the vacuum tank on a special test bench for testing. The heat transfer from the hot end to the cold end can be regarded as one-dimensional axial heat conduction. From the three temperature measurement points of the cold end, the temperature value of the cold end at the bonded interface can be obtained by linear fitting. Similarly, the temperature value of the hot end at the bonded interface can be obtained. The difference between the two temperature values is the heat transfer temperature difference of the bonded interface ΔT . $q/\Delta T$ is the thermal contact conductance of the bonded interface.

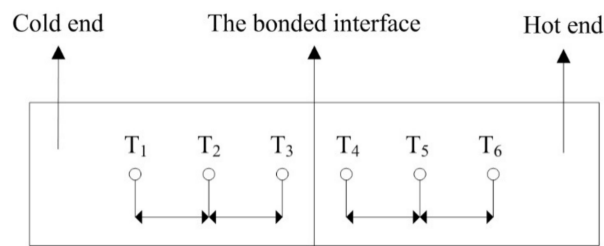


Figure 4. Schematic diagram of the simulation device for thermal property test.

3. Results

3.1. Microstructure of the Joints

The optical microscope image of the joint after bonding for 20 h at 100 °C is presented in Figure 5a. We can see that the thickness of the intermediate layer is uniform at about 120 μm . The intermediate layer can be divided into three parts: the bright yellow circular area is region A, the annular light gray phase around region A is region B, and region C is the near base metal outside region B. There is almost no impurity in region B. There are small striped or spotted dark black phases ($\leq 5 \mu\text{m}$) and small yellow phases in region C.

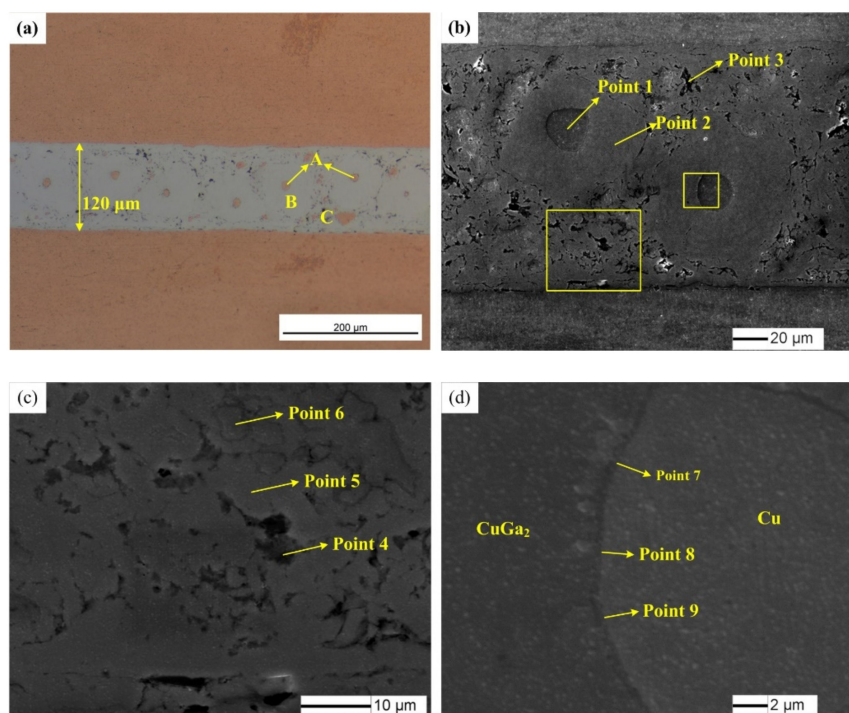


Figure 5. (a) Optical microscope image of the joint after bonding for 20 h at 100 °C; (b–d) SEM images of the joints after bonding for 20 h at 100 °C.

Figure 5b shows the SEM image of the joint after bonding for 20 h at 100 °C. Figure 5c is the magnified picture of the large rectangle in Figure 5b, and Figure 5d is the magnified picture of the small rectangle in Figure 5b. According to the EDS results as shown in Table 1, the yellow circular phase (region A) is unreacted copper wire (point 1) with a diameter of 20 μm . It indicates that about $\frac{3}{4}$ of the copper wire has been consumed. The Ga/Cu atomic ratio of the annular light gray phase (region B) around the copper wire is close to 2:1 (point 2), so may be $\theta\text{-CuGa}_2$ phase, based on the Cu-Ga phase diagram [23,24]. The average Ga/Cu atomic ratio of the striped or spotted dark black phase in region C is 2.415 (point 3 and point 4), and we speculate that it may be $\theta\text{-CuGa}_2$ phase with a small amount of

Ga. As its Ga/Cu atomic ratio is higher than 2, this area may be an accumulation of residual gallium. However, the EDS results show that the content of Ga here is not 100%, which may be caused by the loss of exposed Ga in the polishing process of specimens, given the low melting point and low hardness of Ga. In the intermediate layer, residual Ga is a kind of defect, which is unfavorable to the strength of the joints. Combined with the EDS results, the light gray phase (point 5) in region C should be θ -CuGa₂ phase, and the small yellow phase (point 6) in region C should be copper. From Figure 5d, a thin layer of dark phase can be seen at the copper wire/ θ -CuGa₂ layer interface, and it may be γ_3 -Cu₉Ga₄ phase based on the EDS results and Cu-Ga phase diagram [23,24]. This is consistent with the research that a thin layer of γ_3 -Cu₉Ga₄ is formed at the Cu/CuGa₂ interface [25,26].

Table 1. The EDS analysis results of different points in Figure 5.

Element	Point 1	Point 2	Point 3	Point 4	Point 5	Point 6	Point 7	Point 8	Point 9
Ga	0	66.62	70.26	71.19	67.13	0	34.31	33.02	32.05
Cu	100	33.38	29.74	28.81	32.87	100	65.69	66.98	67.95
atomic ratio of Ga/Cu	–	1.99	2.36	2.47	2.04	–	0.52	0.49	0.47

Ancharov's research shows that [27,28] the only interaction product of copper with gallium is the CuGa₂ at temperatures near 20 °C for more than two days, and there are no other copper–gallium intermetallic compounds. Froemel found [21,29] that the CuGa₂ phase was formed temporarily, then a Cu₉Ga₄ phase was eventually formed; the copper and CuGa₂ had been completely used up and replaced by Cu₉Ga₄ phase with treatment at 200 °C for 80 h. The interfacial reaction products of Cu and Ga are γ_3 -Cu₉Ga₄ and CuGa₂ at 200 °C for 24 h and 148 h [30]. It has been shown that [31–33] the first phase to form is usually the one that contains a higher amount of the fast-diffusing species (i.e., the lower melting point metal). Combined with the Cu-Ga binary phase diagram [23,24], it can be inferred that θ -CuGa₂ phase is formed first, then the γ_3 -Cu₉Ga₄ phase forms by the reaction of θ -CuGa₂ phase and copper with the increase in diffusion temperature or the extension of holding time.

The XRD pattern of the intermediate layer is presented in Figure 6. The results show that the main phases are CuGa₂ phase (the atomic ratio of Ga/Cu is 2), Cu, Ga and Cu₉Ga₄ phase (the atomic ratio of Ga/Cu is 0.44), which further verifies the above analysis results. Therefore, the interaction product of Cu and Ga is mainly θ -CuGa₂ phase, with a little amount of γ_3 -Cu₉Ga₄ phase at the temperature of 100 °C for 20 h.

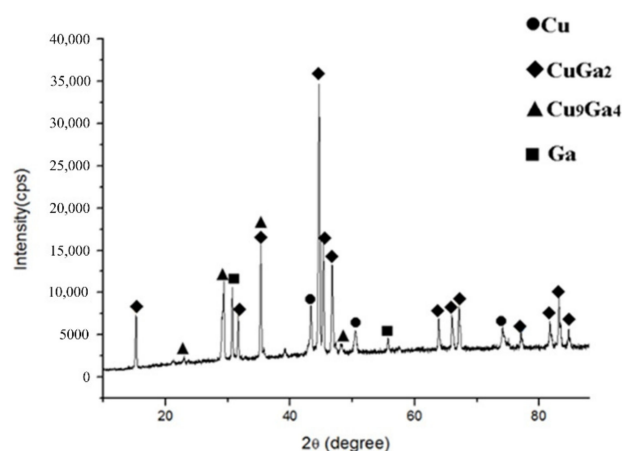


Figure 6. XRD results of the intermediate layer.

Figure 7a–c shows the optical microscope image of the joints at 100 °C with different holding times. From Figure 7a, we can see that the interdiffusion of Cu and Ga is insufficient, as large amounts

of residual copper powder and residual gallium exist at the same time, and the diameter of copper wire is about 25 μm . With the prolongation of holding time, the area of region C and the quantity of residual Ga is gradually reduced, and $\theta\text{-CuGa}_2$ phase (region B) increases in quantity. For 30 h (in Figure 7c), the annular $\theta\text{-CuGa}_2$ phases (region B) connect with each other to form a continuous $\theta\text{-CuGa}_2$ layer, and residual Ga mainly concentrates near the base metal, which may be caused by the insufficient diffusion of base metal and liquid Ga. After the annealing treatment of the Cu substrates (in Figure 7d), the residual gallium in region C is reduced significantly, which verifies our above assumption. At this time, the microstructure of the joint is mainly composed of $\theta\text{-CuGa}_2$ phase, and $\theta\text{-CuGa}_2$ has some advantages over other IMCs, including the nearly isotropic thermal expansion and mechanical properties, small Young's modulus and hardness, and increased compliance and softness [34]. Compared with Figure 7b,c, the copper wire diameter changes a little, which indicates that the diffusion reaction becomes slow after a certain time. The reaction layer thickness grows in proportion to the square root of the reaction time [30], and thus grows slow later. As a whole, with the prolongation of the holding time, the number of defects in the joint decreases and the microstructure becomes more uniform.

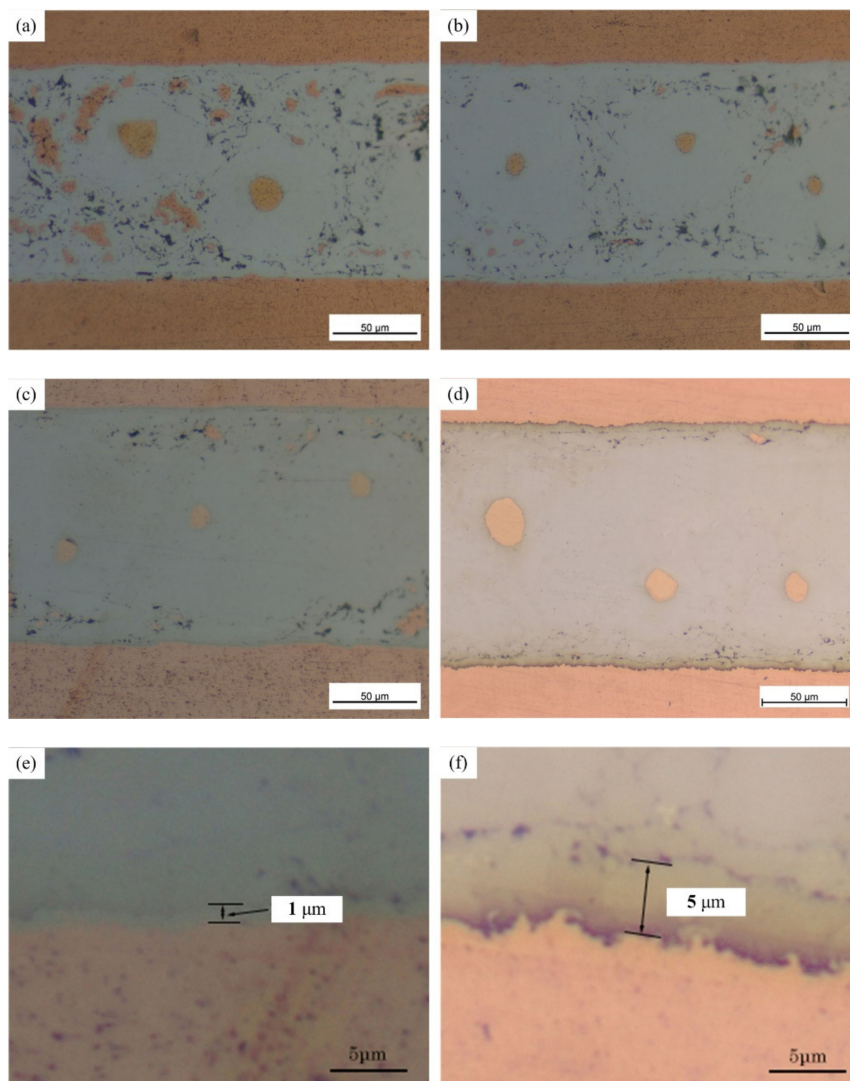


Figure 7. Optical microscope image of the joints at 100 $^{\circ}\text{C}$. (a) Holding time of 10 h; (b) Holding time of 20 h; (c) Holding time of 30 h; (d) After annealing treatment of Cu substrates with holding time of 30 h; (e) Interface between copper substrate and the intermediate layer in Figure 4c; (f) Interface between copper substrate and the intermediate layer in Figure 4d.

Figure 7e,f shows the interface between copper substrate and the intermediate layer with different treatments of the base metal. Without the annealing treatment of Cu substrates, the thickness of the interface is only about 1 μm , and the interface is relatively flat. After annealing, the thickness of the interface is about 5 μm , and the interface is jagged as a mountain peak. The annealing treatment is helpful for the interdiffusion of gallium and the base metal, which is favorable for reducing the defects caused by residual gallium in the intermediate layer.

3.2. Properties of the Joints

Figure 8 shows the variation of shear strength and thermal contact conductance with holding time. The average shear strength and the thermal contact conductance increase gradually with the extension of the holding time. The maximum average shear strength of the joint is 7.9 MPa, and the thermal contact conductance is 88,315 $\text{W}/(\text{m}^2\cdot\text{K})$ with a holding time of 30 h at a bonding temperature of 100 $^{\circ}\text{C}$. The fracture occurs on one side of the copper wire mesh along line A or line B in Figure 9, which is caused by the regular distribution of residual Ga. Residual Ga mainly distributes in region C near the base metal, and uniform $\theta\text{-CuGa}_2$ phase is formed around the copper wire mesh, so region C is the weakest area of the joint. Reducing the size and quantity of residual Ga in the intermediate layer is an effective way to improve the strength of the joints.

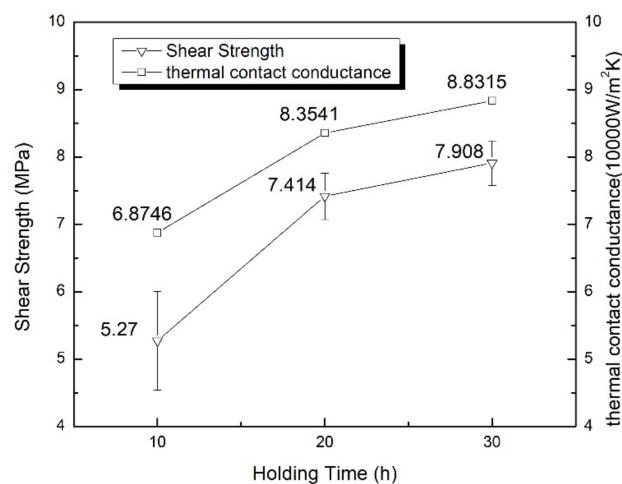


Figure 8. Effect of holding time on shear strength and thermal contact conductance of the joints at the bonding temperature of 100 $^{\circ}\text{C}$.

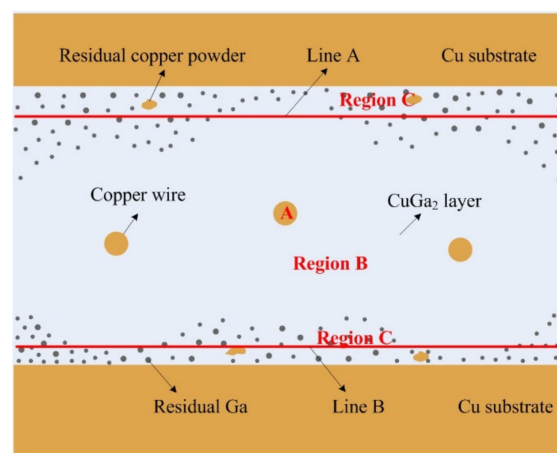


Figure 9. Diagram of fracture location in shear strength test.

The results of the temperature resistance test show that there is no remelting or liquefying phenomenon in the joints with the holding times of 20 h and 30 h, which can meet our requirements. In fact, as the intermediate layer is mainly composed of θ -CuGa₂ phase with a melting point of 254 °C, the joint can surely withstand the temperature of 200 °C when there is only a little residual Ga.

With the prolongation of holding time, the strength and the thermal contact conductance of the joints were improved, which indicated that the thickening of the θ -CuGa₂ layer (region B) and the decrease of residual gallium (region C) were beneficial for the mechanical and thermal properties of the joints. This is because region B is a single θ -CuGa₂ phase with a homogeneous and dense microstructure; region C contains θ -CuGa₂ phase, residual copper powder and residual gallium without a homogeneous and dense microstructure, and there are many interfaces between the different phases. Besides this, the mechanical property of gallium is low. Therefore, the reliability of the joints will not decrease for a long time in service.

4. Discussion

During the heat preservation process, liquid gallium and solid copper wire, and copper powder and copper substrate, interdiffuse and react with each other. The whole process of Cu/Ga SLID bonding is divided into the following three stages:

(1) Pressurization stage—Apply a certain amount of pressure to the joint in the heat preservation process. Liquid Ga is forced to flow into the gap in the copper wire mesh under the pressure to discharge the air mixed in the bonding process, thus the pressure in the interlayer tends to be the same. It can also increase the pressure of the solid/liquid interface, so that the contact between the solid copper and liquid gallium is more sufficient for subsequent diffusion;

(2) Reaction diffusion stage—Driven by a high temperature and concentration gradient, surface diffusion occurred rapidly at the solid Cu/liquid Ga interface to form θ -CuGa₂ phase. The θ -CuGa₂ phase formed due to the fast diffusion kinetics of Cu to liquid gallium [35]. The copper atoms on the solid copper surface diffuse into the surrounding liquid Ga and react rapidly with it to form θ -CuGa₂, as shown in Figure 10a. With the increase in the θ -CuGa₂ compound, θ -CuGa₂ crystals begin to precipitate, as shown in Figure 10b. Then, the θ -CuGa₂ layer gradually forms, as shown in Figure 10c. Above is the formation process of intermetallic compound θ -CuGa₂. After that, the solid copper and liquid gallium are separated by a θ -CuGa₂ layer, and the reaction diffusion will be hindered, as shown in Figure 10d. At this time, the θ -CuGa₂ phase may contain a higher amount of Ga [35].

Froemel thinks [21] that the increased diffusion of the solid phase into the liquid phase leads to a rapid increase of the Cu atoms inside the liquid Ga. After reaching a saturation of solubility, intermetallic compounds are formed, and thus solidification happens. According to the Cu/Ga binary phase diagram [23,24], when the concentration of copper is more than 1%, the liquid's temperature will exceed 100 °C. This means that there will be a solid phase when the concentration of copper is 1~33.3% at 100 °C if the Cu/Ga solution is formed first, which is contrary to the fact. Therefore, in the early stage of the diffusion, the copper atoms react immediately with Ga to form θ -CuGa₂ phase, and do not form the Cu/Ga solution;

(3) Isothermal solidification stage—This stage takes a long time. The main mode of the atoms passing through the θ -CuGa₂ layer is grain boundary diffusion and vacancy diffusion. In the early stage of the θ -CuGa₂ layer formation, the grains grow up gradually, the grain boundary gap is large, most of the grain boundaries are large angle grain boundaries, and the grain boundary energy is high. When the concentration gradient is certain, the activation energy required for copper atoms to cross the grain boundaries is low, which makes it easy to diffuse through the grain boundaries. At the same time, gallium atoms also move across the grain boundaries to the solid copper. At high temperatures, there is a certain concentration of vacancy in the θ -CuGa₂ crystal. Driven by the concentration gradient, copper atoms can also migrate to liquid gallium through vacancy diffusion. In later stages of grain boundary diffusion, vacancy diffusion will play a more important role.

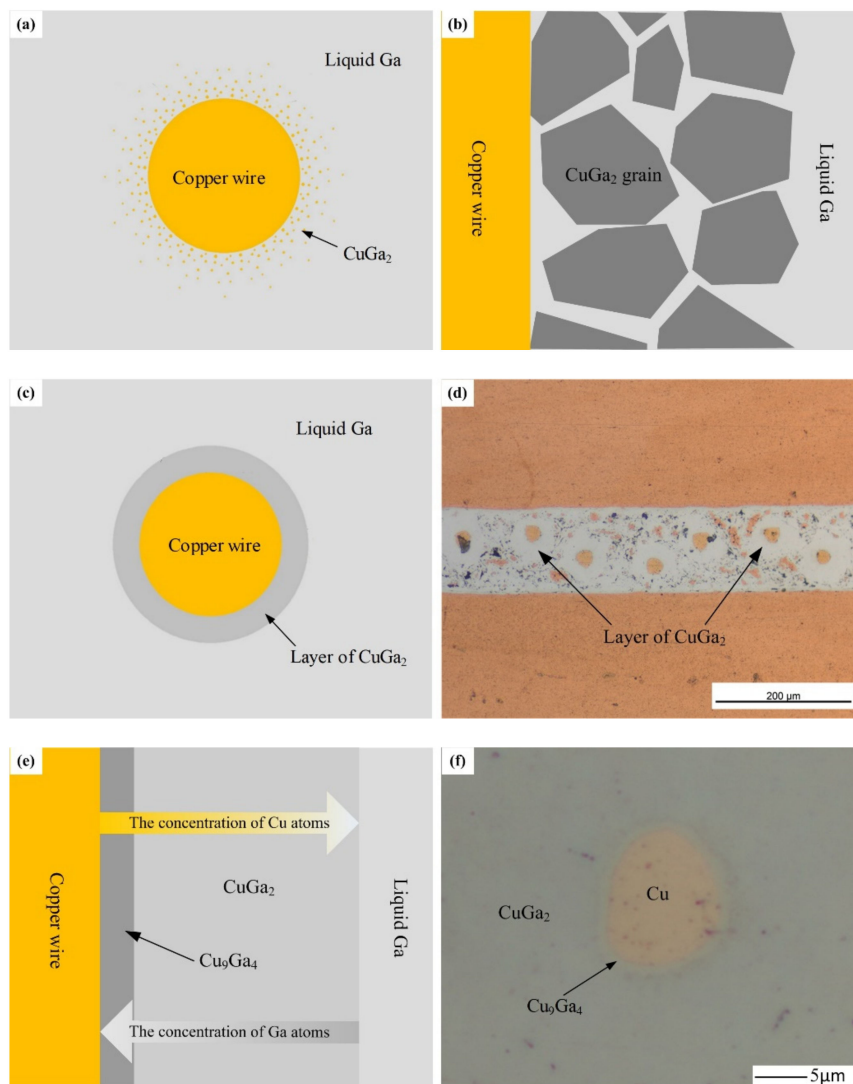


Figure 10. Schematic of the mechanism of Cu/Ga SLID bonding. (a–c) Formation process of intermetallic compound θ -CuGa₂; (d) Formation of θ -CuGa₂ layer; (e) Diffusion of elements in isothermal solidification stage; (f) Formation of thin γ_3 -Cu₉Ga₄ layer.

Copper atoms migrate from the solid copper surface, across the θ -CuGa₂ layer, to liquid gallium by grain boundary diffusion and vacancy diffusion. As shown in Figure 10e, from left to right on the θ -CuGa₂ layer, the concentration of copper atoms decreases gradually, and the concentration of gallium atoms increases gradually. Because the copper atom content in the θ -CuGa₂ layer on the side of the copper wire is relatively high, a new intermetallic compound, γ_3 -Cu₉Ga₄ (2θ -CuGa₂+7Cu = γ_3 -Cu₉Ga₄), is gradually generated. The γ_3 -Cu₉Ga₄ generated is located at the interface of the copper wire and θ -CuGa₂ layer. Then, a thin γ_3 -Cu₉Ga₄ layer is gradually formed as time goes on, as shown in Figure 10f. As the gallium atom content in the θ -CuGa₂ layer on the side of liquid gallium is high, Ga reacts with the diffused copper atom to form θ -CuGa₂. On the micro level, θ -CuGa₂ grains grow and the θ -CuGa₂ grain boundaries become more flat and narrower. On the macro level, the solid–liquid interface advances in the direction of liquid gallium. Ideally, all liquid Ga in the interlayer will be completely transformed into the solid phase if the holding time is long enough.

5. Conclusions

In this work, Cu substrates were successfully bonded using a self-made interlayer at 100 °C without any flux by Cu/Ga SLID bonding. The microstructure, shear strength, temperature resistance and thermal contact conductance of the joints were studied, and the mechanism of Cu/Ga SLID bonding was discussed. This self-made interlayer can be used as a kind of thermal interface material to facilitate interfacial heat transfer. This low temperature metallurgical bonding technology can provide some reference for solving the problem of the heat dissipation of some high-power devices with high reliability. The following conclusions can be drawn:

1. The interfacial microstructure is θ -CuGa₂ phase, residual copper, residual gallium and γ_3 -Cu₉Ga₄ phase. A continuous θ -CuGa₂ layer is formed around the copper wire, which contributes to the main interfacial microstructure. The residual gallium is mainly distributed near the base metal, far away from the copper wire, which is caused by the insufficient interdiffusion of copper substrate and gallium. A thin γ_3 -Cu₉Ga₄ layer is formed at the copper wire/ θ -CuGa₂ layer interface.
2. The interaction product of Cu and Ga is mainly θ -CuGa₂ phase, with only a small amount of γ_3 -Cu₉Ga₄ phase occurring at the temperature of 100 °C for 20 h. With the prolongation of holding time, the θ -CuGa₂ layer thickens, residual Ga decrease, and the microstructure is more uniform.
3. The low-temperature metallurgical bonding of Cu substrates is successfully realized using a self-made interlayer at 100 °C without any flux. The maximum shear strength is 7.9 MPa, the heat-resistant temperature is 200 °C, and the thermal contact conductance is 88,315 W/(m²·K) with a holding time of 30 h at a bonding temperature of 100 °C. The fracture occurs on one side of the copper wire mesh, which is caused by the regular distribution of residual Ga. Region C is the weakest area of the joint. With the prolongation of holding time, the properties of the joints are improved. The thickening of the θ -CuGa₂ layer and reduction in residual gallium are beneficial for the mechanical and thermal properties of the joints.
4. The process of the Cu/Ga SLID bonding can be divided into three stages: pressurization stage, reaction diffusion stage and isothermal solidification stage. In the reaction diffusion stage, Cu reacts with Ga to form θ -CuGa₂ phase, and then a θ -CuGa₂ layer is formed gradually. In the isothermal solidification stage, Cu reacts with θ -CuGa₂ to form γ_3 -Cu₉Ga₄ phase, and a γ_3 -Cu₉Ga₄ layer is gradually formed at the copper wire/ θ -CuGa₂ layer interface; the diffused Cu atoms react with liquid Ga to form θ -CuGa₂, which thickens the θ -CuGa₂ layer on the liquid Ga side.

Author Contributions: Conceptualization, W.Q. and H.Z. (Hongshou Zhuang); methodology, W.Q. and G.M.; validation, W.Q. and Y.Z.; formal analysis, W.Q. and G.M.; investigation, G.M. and H.Z. (Haiyun Zhu); resources, G.M. and H.Z. (Haiyun Zhu); data curation, G.M.; writing—original draft preparation, G.M.; writing—review and editing, W.Q. and Y.Z.; supervision, W.Q. and Y.Z.; project administration, W.Q.; funding acquisition, W.Q. All authors have read and agreed to the published version of the manuscript.

Funding: This project was funded by key special projects of the national key R&D program (2017YFB0305700).

Acknowledgments: All the authors of this paper sincerely thank the teachers of the testing center of the school of materials science and engineering in Beihang university, and the China academy of space technology for their help in performance testing. This work was supported by key special projects of the national key R&D program (2017YFB0305700).

Conflicts of Interest: The authors declare no conflict of interest.

References

1. Belhardja, S.; Mimounia, S.; Saidanea, A.; Benzohra, M. Using microchannels to cool microprocessors: A transmission-line-matrix study. *Microelectron. J.* **2003**, *34*, 247–253. [[CrossRef](#)]
2. Yeh, L.T. Review of heat transfer technologies in electronic equipment. *J. Electron. Packag. Trans. ASME* **1995**, *117*, 333–339. [[CrossRef](#)]

3. Moore, A.L.; Shi, L. Emerging challenges and materials for thermal management of electronics. *Mater. Today* **2014**, *17*, 163–174. [[CrossRef](#)]
4. Ebadian, M.A.; Lin, C.X. A review of high-heat-flux heat removal technologies. *J. Heat Transf.* **2011**, *133*, 110801. [[CrossRef](#)]
5. Gwinn, J.P.; Webb, R.L. Performance and testing of thermal interface materials. *Microelectron. J.* **2003**, *34*, 215–222. [[CrossRef](#)]
6. Hansson, J.; Torbjörn, M.J.N.; Ye, L.L.; Liu, J. Novel nanostructured thermal interface materials: A review. *Int. Mater. Rev.* **2017**, *63*, 22–45. [[CrossRef](#)]
7. Mei, Y.H.; Wang, T.; Cao, X.; Chen, G.; Lu, G.Q.; Chen, X. Transient Thermal Impedance Measurements on Low-Temperature-Sintered Nanoscale Silver Joints. *J. Electron. Mater.* **2012**, *41*, 3152–3160. [[CrossRef](#)]
8. Bai, J.G.; Zhang, Z.Z.; Calata, J.N.; Lu, G. Low-Temperature Sintered Nanoscale Silver as a Novel Semiconductor Device-Metallized Substrate Interconnect Material. *IEEE Trans. Compon. Packag. Technol.* **2006**, *29*, 589–593. [[CrossRef](#)]
9. Fu, S.C.; Mei, Y.H.; Lu, G.Q.; Li, X.; Chen, G.; Chen, X. Pressureless sintering of nanosilver paste at low temperature to join large area ($\geq 100 \text{ mm}^2$) power chips for electronic packaging. *Mater. Lett.* **2014**, *128*, 42–45. [[CrossRef](#)]
10. Chen, G.; Yu, L.; Mei, Y.H.; Li, X.; Chen, X.; Lu, G.Q. Uniaxial ratcheting behavior of sintered nanosilver joint for electronic packaging. *Mater. Sci. Eng. A* **2014**, *591*, 121–129. [[CrossRef](#)]
11. Yan, J.F.; Zou, G.S.; Wu, A.P.; Ren, J.L.; Yan, J.C.; Hu, A.M.; Zhou, Y. Pressureless bonding process using Ag nanoparticle paste for flexible electronics packaging. *Scr. Mater.* **2012**, *66*, 582–585. [[CrossRef](#)]
12. Wang, S.A.; Li, M.Y.; Ji, H.J.; Wang, C.Q. Rapid pressureless low-temperature sintering of Ag nanoparticles for high-power density electronic packaging. *Scr. Mater.* **2013**, *69*, 789–792. [[CrossRef](#)]
13. Youssef, T.; Rmili, W.; Woïrgard, E.; Azzopardi, S.; Vivet, N.; Martineau, D.; Meuret, R.; Quilliec, G.L.; Richard, C. Power modules die attach: A comprehensive evolution of the nanosilver sintering physical properties versus its porosity. *Microelectron. Reliab.* **2015**, *55*, 1997–2002. [[CrossRef](#)]
14. Sun, L.; Chen, M.H.; Zhang, L.; He, P.; Xie, L.S. Recent progress in SLID bonding in novel 3D-IC technologies. *J. Alloys Compd.* **2020**, *818*, 152825. [[CrossRef](#)]
15. Jung, D.H.; Sharma, A.; Mayer, M.; Jung, J.P. A review on recent advances in transient liquid phase (TLP) bonding for thermoelectric power module. *Rev. Adv. Mater. Sci.* **2018**, *53*, 147–160. [[CrossRef](#)]
16. Matsushita, M.; Sasaki, Y.; Ikuta, Y. Investigation of a New Sn–Cu–Ga Alloy Solder. *Defect Diffus. Forum* **2011**, *312*, 518–523. [[CrossRef](#)]
17. Liu, S.; Sweatman, K.; McDonald, S.; Nogita, K. Ga-Based Alloys in Microelectronic Interconnects: A Review. *Materials* **2018**, *11*, 1384. [[CrossRef](#)]
18. Ramm, P.; Lu, J.J.Q.; Taklo, M.M.V. Thermocompression Cu–Cu Bonding of Blanket and Patterned Wafers. In *Handbook of Wafer Bonding*; Wiley-VCH Verlag & Co. KGaA: Weinheim, Germany, 2012; pp. 161–163.
19. Frömel, J.; Lin, Y.C.; Wiemer, M.; Gessner, T.; Esashi, M. Low temperature metal interdiffusion bonding for micro devices. In Proceedings of the 2012 3rd IEEE International Workshop on Low Temperature Bonding for 3D Integration, Tokyo, Japan, 22–23 May 2012; p. 163.
20. Marinković, Ž.; Simić, V. Comparative analysis of interdiffusion in some thin film metal couples at room temperature. *Thin Solid Film* **1992**, *217*, 26–30. [[CrossRef](#)]
21. Froemel, J.; Baum, M.; Wiemer, M.; Gessner, T. Low-temperature wafer bonding using solid-liquid inter-diffusion mechanism. *J. Microelectromech. Syst.* **2015**, *24*, 1973–1979. [[CrossRef](#)]
22. Lin, S.K.; Chang, H.M.; Cho, C.L.; Liu, Y.C.; Kuo, Y.K. Formation of solid-solution Cu-to-Cu joints using Ga solder and Pt under bump metallurgy for three-dimensional integrated circuits. *Electron. Mater. Lett.* **2015**, *11*, 687–694. [[CrossRef](#)]
23. Ma, C.; Xue, S.; Wang, B. Study on novel Ag-Cu-Zn-Sn brazing filler metal bearing Ga. *J. Alloys Compd.* **2016**, *688*, 854–862. [[CrossRef](#)]
24. Li, J.B.; Ji, L.N.; Liang, J.K.; Zhang, Y.; Luo, J.; Li, C.R.; Rao, G.H. A thermodynamic assessment of the copper–gallium system. *Calphad* **2008**, *32*, 447–453. [[CrossRef](#)]
25. Liu, S.; Zeng, G.; Yang, W.; McDonald, S.; Gu, Q.; Matsumura, S.; Nogita, K. Interfacial Reactions between Ga and Cu-10Ni Substrate at Low Temperature. *ACS Appl. Mater. Interfaces* **2020**, *12*, 21045–21056. [[CrossRef](#)] [[PubMed](#)]

26. Lin, S.K.; Cho, C.L.; Chang, H.M. Interfacial Reactions in Cu/Ga and Cu/Ga/Cu Couples. *J. Electron. Mater.* **2013**, *43*, 204–211. [[CrossRef](#)]
27. Ancharov, A.I.; Grigoryeva, T.F.; Barinova, A.P.; Boldyrev, V.V. Interaction between copper and gallium. *Russ. Metall. (Met.)* **2008**, *2008*, 475–479. [[CrossRef](#)]
28. Ancharov, A.I.; Grigoryeva, T.F. Investigation of the mechanism of interaction between reagents in alloys based on Cu-Ga system. *Nucl. Instrum. Methods Phys. Res. A* **2005**, *543*, 139–142. [[CrossRef](#)]
29. Froemel, J.; Baum, M.; Wiemer, M.; Gessner, T. Solid liquid inter-diffusion bonding at low temperature. In Proceedings of the 2014 4th IEEE International Workshop on Low Temperature Bonding for 3D Integration (LTB-3D), Tokyo, Japan, 15–16 July 2014; p. 62.
30. Chen, S.W.; Lin, J.M.; Yang, T.C.; Du, Y.H. Interfacial Reactions in the Cu/Ga/Co and Cu/Ga/Ni Samples. *J. Electron. Mater.* **2019**, *48*, 3643–3654. [[CrossRef](#)]
31. Cardellini, F.; Contini, V.; Mazzone, G.; Vittori, M. Phase Transformations and chemical reactions in mechanically alloyed Cu/Zn powders. *Scr. Metall. Mater.* **1993**, *28*, 1035–1038. [[CrossRef](#)]
32. Pabi, S.K.; Joardar, J.; Murty, B.S. Formation of nanocrystalline phases in the Cu-Zn system during mechanical alloying. *J. Mater. Sci.* **1996**, *31*, 3207–3211. [[CrossRef](#)]
33. Pretorius, R.; Theron, C.C.; Vantomme, A.; Mayer, J.W. Compound Phase Formation in Thin Film Structures. *Crit. Rev. Solid State Mater. Sci.* **1999**, *24*, 1–62. [[CrossRef](#)]
34. Liu, S.; Yang, W.; Kawami, Y.; Gu, Q.; Matsumura, S.; Qu, D.; McDonald, S.; Nogita, K. Effects of Ni and Cu Antisite Substitution on the Phase Stability of CuGa₂ from Liquid Ga/Cu-Ni Interfacial Reaction. *ACS Appl. Mater. Interfaces* **2019**, *11*, 32523–32532. [[CrossRef](#)] [[PubMed](#)]
35. Hong, S.J.; Suryanarayana, C. Mechanism of low-temperature θ -CuGa₂ phase formation in Cu-Ga alloys by mechanical alloying. *J. Appl. Phys.* **2004**, *96*, 6120–6126. [[CrossRef](#)]



© 2020 by the authors. Licensee MDPI, Basel, Switzerland. This article is an open access article distributed under the terms and conditions of the Creative Commons Attribution (CC BY) license (<http://creativecommons.org/licenses/by/4.0/>).